

Vibrational and stochastic resonances in two coupled overdamped anharmonic oscillators

V. M. Gandhimathi^a, S. Rajasekar^a, J. Kurths^b

^a School of Physics, Bharathidasan University,
Tiruchirappalli-620 024, Tamilnadu, India

^b Institut für Physik, Potsdam Universität,
Am Neuen Palais 10, D-14469 Potsdam, Germany

E-mail: S. Rajasekar: rajasekar@physics.bdu.ac.in

V. M. Gandhimathi: vm_gandhimathi@yahoo.co.in

J. Kurths: jkurths@agnld.uni-potsdam.de

Abstract

We study the overdamped version of two coupled anharmonic oscillators under the influence of both low- and high-frequency forces respectively and a Gaussian noise term added to one of the two state variables of the system. The dynamics of the system is first studied in the presence of both forces separately without noise. In the presence of only one of the forces, no resonance behaviour is observed, however, hysteresis happens there. Then the influence of the high-frequency force in the presence of a low-frequency, i.e. biharmonic forcing, is studied. Vibrational resonance is found to occur when the amplitude of the high-frequency force is varied. The resonance curve resembles a stochastic resonance-like curve. It is maximum at the value of g at which the orbit lies in one well during one half of the drive cycle of the low-frequency force and in the other for the remaining half cycle. Vibrational resonance is characterized using the response amplitude and mean residence time. We show the occurrence of stochastic resonance behaviour in the overdamped system by replacing the high-frequency force by Gaussian noise. Similarities and differences between both types of resonance are presented.

PACS : 02.50.-r; 05.40.-a; 05.45.-a

Keywords: Vibrational resonance; low-frequency force; high-frequency force; stochastic resonance; noise; mean residence time.

1. Introduction

Stochastic resonance (SR) [1-4] occurs when a weak periodic signal in a nonlinear system is amplified by a noise of appropriate strength. In bistable systems, it has been shown that other types of external driving can mimic the role of noise in the amplification of the signal. Such external drivings include a chaotic signal [5] or a high-frequency periodic force [6]. In the latter case, the system is driven by a biharmonic signal, consisting of a low-frequency and a high-frequency periodic force. Landa and McClintock studied the effect of high-frequency force. They found a resonance-like behaviour in the response of the system at the frequency of the low-frequency periodic force, when the amplitude of the high-frequency force passed through a critical value and is termed as vibrational resonance (VR). After this seminal work VR has been studied in a bistable oscillator [7], a Duffing oscillator [8], excitable systems [9] and spatially extended systems [10]. Experimental evidences of VR in a vertical cavity surface emitting laser [11], simple electronic circuit [9] and in an overdamped Duffing oscillator [12] have been reported.

The study of two-frequency signals is important in communication because usually a low-frequency signal modulates a high-frequency carrier signal and is also an object of interest in many other branches of physics and biology such as lasers [13], acoustics [14], neuroscience [15] and ionosphere [16]. Practical importance especially in medicine of a high-frequency force has been reported [17-20].

In this paper we study a multistable system, i.e. a more generalized one compared to former investigations, under the influence of a biharmonic force and noise. This enables to study VR as well as SR and compare their characteristic features in the system

$$\ddot{x} = -a_1x - bx^3 + xy^2 + f \sin \omega_1 t + g \sin \omega_2 t + \xi(t); \quad (1a)$$

$$\ddot{y} = -a_2y - by^3 + x^2y; \quad (1b)$$

The terms $f \sin \omega_1 t$ and $g \sin \omega_2 t$ are the low-frequency signal of amplitude f and high-frequency ($\omega_2 \gg \omega_1$) signal of amplitude g . System (1) is an overdamped version of two

coupled anharmonic oscillators. Its potential in the absence of damping and external drivings is given by

$$V(x; y) = \frac{a_1}{2}x^2 + \frac{b_1}{4}x^4 - \frac{a_2}{2}y^2 + \frac{b_2}{4}y^4 - \frac{1}{2}x^2y^2: \quad (2)$$

In a very recent work, Baxter and McKane [21] considered eqs (1) as a model for competition between two species. We fix the parameters of the system as $a_1 = 1.0$, $a_2 = 1.1$, $b_1 = 1.0$, $b_2 = 1.0$, $\gamma = 0.01$. For this choice, the potential is a four-well potential. Figure (1) shows the 3-dimensional plot of the four-well potential. The potential wells are designated as V_{++} for $x > 0, y > 0$; V_{+-} for $x > 0, y < 0$; V_{-+} for $x < 0, y > 0$; V_{--} for $x < 0, y < 0$. is additive white noise with $\langle \xi(t) \xi(s) \rangle = D \delta(t - s)$ and D is the noise intensity.

The outline of the paper is as follows. In section 2 we discuss the response of the system (1) in the presence of a low-frequency periodic force only ($g = 0; D = 0$) respectively a high-frequency periodic force only ($f = 0; D = 0$). In the presence of only one of these forces, periodic orbits of the system (1) with a period equal to the single applied force are found to exist. Chaos is not observed at all. We find that a cross-well orbit is realized above a critical amplitude of the external driving. In section 3 we consider the noise free system with both low- and high-frequency forces. We describe the occurrence of VR and characterize it using the response amplitude and mean residence time. In section 4 we show the occurrence of SR in the presence of noise and in the absence of high-frequency force. We discuss the similarities and differences between VR and SR. Finally, section 5 contains our conclusions.

2. Influence of only one periodic forcing

Before studying the system (1) in the presence of both, low- and high-frequency forces, we consider the noise free system with the low-frequency force alone ($g = 0$) respectively the high-frequency force alone ($f = 0$). Though the potential has four wells, there is oscillating behaviour only in the wells V_{++} and V_{--} , while the other two wells V_{+-} and V_{-+} are stationary, since the periodic forces are added only to the x-component of the system (1).

When the forces and noise are included, a jumping of orbits between only the wells V_{++} and V_{+-} is observed for a range of control parameters considered in the present study. Therefore, we restrict ourselves to the motion confined to the wells V_{++} and V_{+-} .

We start with a low-frequency forcing. For a fixed ϵ and for small values of f , two periodic orbits one in the well V_{++} and another one in the well V_{+-} exist now. The size of the orbits is found to increase with increasing f . At a critical value f_c of f , after transient evolution the trajectory of the system resides in one of the two potential wells, for example, say, V_{++} for a certain interval of time and enters into the other well, say, V_{+-} and stays there for some time and the above process repeats. That is, the trajectory traverses both the potential wells. The x -component of the system changes from positive to negative and then to positive and so on whereas the sign of y remains same. This type of jumping between two or more wells is termed as cross-well motion. For $\epsilon = 0.1$, we find $f_c = 0.427$ as seen in the bifurcation diagram, Fig 2. In this and in the other bifurcation diagrams the ordinate represents the values of $x(t)$ collected at time t equal to every integral multiples of $2/\epsilon$ (Poincare points) after leaving sufficient transient evolution. Figure 2 (a) is obtained by varying the amplitude f from a small value in the forward direction. For the starting value of f , the initial condition is chosen such that after some transient the orbit is confined to the well V_{++} only. For the other values of f , the last state of the system corresponding to the previous value of f is chosen as the initial condition. In Fig 2 (a) at $f = f_c = 0.427$, the x value suddenly jumps to a negative value. Figure 2 (b) is obtained by varying f in the reverse direction from the value 2. Different paths are followed in the Figs 2 (a) and 2 (b). That is, the system exhibits hysteresis when the control parameter f is varied smoothly from a small value to a large one and then back to a small value. By numerical simulations we find that f_c scales as $f_c = A\epsilon^{0.75} + B$ and is valid for ϵ in the range 0.01 to 1.0. The values of A and B are 0.754 and 0.409 respectively. That is, f_c increases with increasing ϵ .

The bifurcation diagram and the Lyapunov exponents are calculated for f in the range

[0,20]. Period doubling bifurcations and chaotic dynamics are not observed here but there is only a stable periodic orbit of period $T = 2\pi$.

Next, we consider the system (1) in the presence of the high-frequency force alone, that is $f = 0; D = 0$. The amplitude g of the high-frequency force is varied in the forward as well as reverse directions for $\epsilon = 5$ and the bifurcation diagrams are plotted (Fig.3). Here again we find a cross-well motion at a critical value $g_c = 3.24$ of the force and a hysteresis. Chaotic behaviour is again not observed. g_c is numerically calculated for various values of ϵ and is found to increase with increasing ϵ . The calculated g_c scales as $g_c = C + D\epsilon$ where $C = 0.5$ and $D = 0.298$, i.e., g_c varies linearly with ϵ . g_c is valid for ϵ in the range 0.01 to 10.

3. Vibrational resonance

In the previous section, we studied the effect of the low-frequency force and the high-frequency force separately in the system (1). Now, we consider the effect of the high-frequency force on the response of the system in the presence of the low-frequency force ($f \neq 0; g \neq 0$) but in the noise-free case ($D = 0$).

A. Hysteresis

We set $f = 0.2, \epsilon = 0.1$ and $\epsilon = 5$. For these values of the parameters, in the absence of the high-frequency force ($g = 0$), we get $f_c = 0.427$. For $f = 0.2$ in the absence of the high-frequency force there is no cross-well motion, i.e. the low-frequency force alone is not sufficient to induce a cross-well motion. We now study the response of the system by varying the amplitude g of the high-frequency force. For $g < g_c = 2.67$ two periodic orbits with the same period $T = 2\pi$ one in the well V_{++} and another in the well V_{+-} occur. For $g > g_c$ the two periodic orbits merge and form a cross-well orbit. Figures 4(a) and 4(b) show the bifurcation diagrams obtained by varying g in the forward and reverse directions respectively. We can clearly notice a hysteresis.

B. Response amplitude Q and mean residence time

In addition to the hysteresis, system (1) exhibits also the phenomenon of VR when g is varied. To quantify the occurrence of VR, we use the response amplitude Q of the system at the signal frequency ω . It is defined as [6] $Q = \sqrt{Q_s^2 + Q_c^2}$ with

$$Q_s = \frac{2}{nT} \int_0^{nT} x(t) \sin(2\pi t/T) dt; \quad Q_c = \frac{2}{nT} \int_0^{nT} x(t) \cos(2\pi t/T) dt; \quad (3)$$

where T is the period of the response and n is an integer. We numerically calculate Q with a low-frequency force only, a high-frequency force only and with both forces. In the case of $f = 0$, the response amplitude is measured as $Q = \sqrt{Q_s^2 + Q_c^2}$. Q_s and Q_c measure the coefficients of the Fourier sine and cosine components respectively of the output signal at the frequency $2\pi/T$. Q measures the amplitude of the response at the frequency $2\pi/T$. When the system is driven by only one force, the response Q monotonically increases with the amplitude f respectively g of the corresponding driving force. This is shown in Fig.5 (a) for $g = 0; \omega = 0.1$ and in Fig.5 (b) for $f = 0; \omega = 5.0$. Figure (6) shows a completely different result when both forces are switched on. As g increases, the resultant amplitude Q increases and reaches a maximum value at $g = g_{max} = 2.98$ but then decreases with further increase in g . This phenomenon is the VR, since the occurrence is due to high-frequency force. We first describe both qualitatively and quantitatively the VR and then compare it with the well-known phenomenon of SR.

The resonance curve in Fig.6 essentially consists of three regions:

Region-I : $0 < g < g_c (= 2.67)$.

Region-II : $g_c \leq g \leq g_{max} (= 2.98)$.

Region-III : $g > g_{max}$.

Figures (7) and (8) show the phase portraits and trajectory plots for a few values of g in the interval $[0, 6]$. In all the three regions the motion is periodic with the period $T = 2\pi/\omega$. For $0 < g < g_c = 2.67$, that is in region-I, each periodic orbit is confined only to one well. There is no cross-well motion (cf. Figs.7 (a-b) for $g = 1.0$ and 2.5). In region-I, the

amplitude Q increases smoothly and slowly with g . At $g_c = 2.67$, a cross-well motion is initiated. Figures 7(c) and 7(d) show the coexistence of two such orbits for $g = 2.67$. In Fig.7(c) the period- T orbit spends relatively a very small amount of time in the region $x > 0$, that is in the well V_{++} . In contrast to this, the orbit in Fig.7(d) traverses only a small region and relatively a very small time in the well V_{-+} . In all subplots of Fig.7, the state variable y is always positive.

We also calculate the mean residence time τ_{MR} spend in the wells V_{++} and V_{-+} by the orbit for g in the interval $[g_c; 6]$. In our numerical calculation of τ_{MR} for $g = g_c$ we have chosen initial conditions such that the orbit spending most of the time in the well V_{++} . Figure 9(a) shows the plot of $\ln(\tau_{MR})$ versus $1/(g - g_c)$ in the well V_{++} and Fig.9(b) in the well V_{-+} . The barrier heights for the path $V_{++} \rightarrow V_{-+}$ and $V_{-+} \rightarrow V_{++}$ are the same. At $g = g_c$, τ_{MR} of the orbit in the well V_{-+} is very small while for V_{++} it is close to $T = 2\pi$. As g increases, τ_{MR} in V_{++} decreases rapidly, while τ_{MR} in V_{-+} increases rapidly. As $g \rightarrow g_{max}$ (which is denoted by X in Fig.9), τ_{MR} in the well V_{++} decreases to $T=2$, while τ_{MR} in V_{-+} increases to $T=2$. At $g = g_{max}$ the orbit lies in the well V_{++} during one half of the drive cycle of the lower frequency and in the well V_{-+} in the other half of the cycle as shown in Figs.7(e) and 8(d). The above dynamics is in region-II. In this region, there is a rapid increase in the amplitude Q and region-II is very narrow.

Though the period of the orbit in the region-III is still T , the form of the orbit is different from those in the regions I and II. Figure 7(f) depicts the phase portrait of the period- T orbit for $g = 6.0$. The corresponding trajectory plot is shown in Fig.8(f). These two figures can be compared with the phase portrait and trajectory plot of orbits in the regions I and II. The orbit appears to move on a '1' shaped surface. When g is increased above g_{max} , the mean residence time of the orbit in the potential well V_{++} and in the well V_{-+} decreases. This is evident from the trajectory plots, Fig.8(e) and 8(f). In the region-III Q decreases much slower than it increases in region-II. From the above, we find that as g is increased from g_c , τ_{MR} of the orbit in the well V_{++} decreases from T , becomes $T=2$ at $g = g_{max}$ and

then decreases with further increase in g . For the well V_+ , when g is increased from g_c , the value of \dot{M}_R increases from zero, reaches the maximal value $T=2$ at $g = g_{max}$ and then decreases for $g > g_{max}$.

We study the dependence of Q on the frequencies ω and γ of the driving forces. In Fig.10 (a), $Q(g)$ is plotted for different values of ω , namely $\omega = 0.1, 0.25, 0.5$ and with $\gamma = 5, f = 0.2$. With increasing ω , Q_{max} decreases. The value of g_{max} (at which Q is maximum) is also found to depend on ω . The resonance peak becomes more and more sharp with decreasing ω . In Fig.10 (b) the resonance curve is plotted for different values of γ for $\omega = 0.1$. Q_{max} is almost the same in all the cases. But g_{max} and the width of the resonance curve increases with γ .

We have studied the effect of high-frequency force with and without hysteresis phenomenon. For example, for $a_1 = 1.0, a_2 = 1.1, b_1 = 1.0, b_2 = 1.0, \gamma = 0.01$, the potential of the system is a single-well and the bifurcation diagram for $f \in [0; 50]$ show the absence of hysteresis behaviour. The parameter g is varied for several fixed values of f in the above specified interval for $\gamma = 5.0$. In all the cases vibrational resonance is not observed. Recently, Ullner et al [9] analysed the effect of high-frequency forcing in excitable systems which have only one stable fixed point but perturbations above a certain threshold induce large excursions of the form of spikes in phase space. The duration of those excursions introduced an intrinsic time scale and the excitable systems exhibited vibrational resonance to the high-frequency harmonic driving.

The VR curve closely resembles the SR curve. In VR the role of noise is played in some sense by the high-frequency force. There are some characteristic similarities and differences between these two phenomena which will be discussed in the next section.

4. Stochastic resonance

In this section, we replace the high-frequency force in eq (1) by the noise term $\xi(t)$ and

show the occurrence of SR. Then we make a brief comparison of VR with SR. Noise is added to the state variable x as $x_{i+1} = x_i + \Delta t \left(\frac{P}{D} + \xi(t) \right)$ with $\xi(t) = \frac{P}{D} \xi(t)$ after each integration step Δt . $\xi(t)$ represents Gaussian random numbers with zero mean, unit variance and D is the intensity of the noise. In our numerical simulation we integrate the equation of motion with a time step $\Delta t = (2\pi) = 2000$. The parameters in eqs (1) are fixed as $a_1 = 1.0$, $a_2 = 1.1$, $b_1 = 1.0$, $b_2 = 1.0$, $\gamma = 0.01$, $f = 0.2$, $\omega = 0.1$ and $g = 0$.

Figure 11(a) shows the numerically computed signal-to-noise ratio ($SNR = 10 \log_{10}(S/N)$ dB) as a function of the noise intensity D . Here S and N are the amplitudes of the signal peak and the noise background respectively. S is read directly from the power spectrum at the frequency ω of the driving periodic force. To calculate the background of the power spectrum around ω , we consider the power spectrum in the interval $[\omega - \Delta\omega, \omega + \Delta\omega]$ after subtracting the point namely ω representing the SR spike. The average value of the power spectrum in the above interval is taken as background noise level at ω . In addition to the SNR plot, the response amplitude Q is measured by varying the noise intensity D . Figure 11(b) shows the variance of Q against noise intensity D . Figure (12) shows x vs t for four values of noise intensity D . The dependence of M_R on D is depicted in Fig.13. These three figures can be compared with the Figs.(6), (8) and (9) for VR. As in the Q vs g response for VR, we find in Fig.11(a) and (b) again three regions, here in dependence on the noise strength D . The value of D at which the response is maximum is found to be the same in both SNR as well as Q plot.

However there are also strong differences between VR and SR; mainly to mention the following ones: In the D region-I, similar to the region-I in Fig.6, orbits confined to a single-well alone exist. At $D = D_c = 0.022$, a noise-induced cross-well motion is initiated. At D_c , M_R in the well V_{++} is estimated as 700. M_R in the well V_{-+} is also 700. This value of M_R at D_c is much higher than the period $T = 2\pi$ of the driving force. In contrast, for the high-frequency induced oscillatory dynamics (see Fig.9) M_R for V_{++} at g_c is T , while it is very small for V_{-+} .

In the case of noise-induced dynamics, M_R decreases for both wells V_{++} and V_{+-} and is identical in both. But in the case of the high-frequency induced dynamics, M_R of V_{++} decreases from T , whereas that of V_{+-} increases from a small value with the amplitude g . In Fig.12 the maximum of SNR is realized for $D = D_{max} = 0.32$ at which $M_R = T=2$. In Fig.12 (c), an almost periodic switching between the positive and negative values of x is clearly seen at D_{max} . In Fig.6 Q becomes maximum at $g = g_{max} = 2.98$ at which $M_R = T=2$. In region-III for the wells V_{++} and V_{+-} , M_R decreases with increase in D . For large noise the motion is dominated by the noise term and the trajectory jumps erratically between both wells. In the case of the high-frequency induced dynamics also in region-III, for large values of amplitude g , the motion is dominated by the high-frequency force which is evident in Fig.8 (f).

Though the potential $V(x;y)$, eq (2), built up a four-well potential with the fixed parameters, only two of them determine the dynamics and are sufficient for the vibrational and stochastic resonance effects. This is because both the forces are added to the x -component of the system only. That is, the applied harmonic forces make only the potential wells V_{++} and V_{+-} to oscillate while the other two wells V_{--} and V_{-+} remain stationary. Consequently, the VR and SR effects are confined to the two wells V_{++} and V_{+-} only. The addition of external periodic forcings to both state variables induces transitions between all the wells. We note that eq (1) decouples into two single oscillators for the parametric choices $a_2 = a_1$, $b_2 = b_1$, $\gamma = 3\eta$ under the change of variables $x = u + v$ and $y = u - v$. Only for these specific parametric choices it is enough to consider a one-dimensional double-well potential system instead of the system (1). The values of parameters considered in our present study are different from the above special choice. Both the one-dimensional double-well potential system and two-dimensional four-well potential system are capable of showing VR and SR phenomena. However, the critical values of the parameters at which they occur will be different in both systems due to the coupling term. We cannot infer about the dynamics of the two-dimensional four-well potential system from the study of a one-dimensional double-well

potential system .

5. Conclusion

In this paper we have discussed the phenomenon of vibrational resonance in a multistable system under the action of a two frequency signal, where one frequency is much larger than the other. Adding the high-frequency force to the system , which is already driven externally by the low-frequency one, results in the amplification of the low-frequency signal. The response amplitude curve resembles the SR profile. Therefore, we have also studied stochastic resonance by replacing the high-frequency term with a Gaussian noise term . By comparing both VR and SR , the similarities and differences between both are studied. The major results of our present work are the following:

- (i) Vibrational resonance is found to occur only in the presence of hysteresis for the given choice of parameters.
- (ii) In both VR and SR , the maximum response is obtained only when the mean residence time is half of the period of the driving force $f \sin \omega t$.
- (iii) The variation of the mean residence time with the amplitude of the high-frequency force in VR is found to be different from that of it with the amplitude of noise in SR .
- (iv) In the high-frequency force induced VR , the mean residence time τ_{MR} in the well V_{++} decreases from T , while there is an increase in τ_{MR} in the well V_{+-} from a small value. In contrast, in SR τ_{MR} in the wells V_{++} and V_{+-} are identical and decreases with the increase in the amplitude of the noise.
- (v) The SNR and the response amplitude Q both peaks at the same value of D at which $\tau_{MR} = T/2$. This suggests that in addition to SNR one can also use the quantity Q to characterize SR .

Recently, we have found that for the external force in the form of the modulus of a sine wave and a rectified sine wave, the maximum SNR is obtained only when the sum of the residence times of both wells is $T=2$ [22]. Therefore, it is interesting to study in future VR

with different periodic forces especially with the above two forces and generalize the concept of mean residence time at the maximum output. We expect experimental verifications in lasers, circuits etc, but also applications in ecology and biology.

Acknowledgement

The work of SR forms part of a Department of Science and Technology, Government of India research project (VMG and SR). JK acknowledges the support from his Humboldt-C SIR research award. The authors acknowledge helpful suggestions of anonymous referees.

REFERENCES

- [1] P. Jung, *Phys. Rep.* 234 (1993) 175.
- [2] K. Wiesenfeld, F. Jaramillo, *Chaos* 8 (1998) 539.
- [3] L. Gammaitoni, P. Hanggi, P. Jung, K. Marchesoni, *Rev. Mod. Phys.* 70 (1998) 223.
- [4] F. Moss, L. M. Ward, W. G. Sannita, *Clinical Neurophysiology* 115 (2004) 267.
- [5] S. Sinha, *Physica A* 270 (1999) 204.
- [6] P. S. Landa, P. V. E. McClintock, *J. Phys. A: Math. Gen.* 33 (2000) L433.
- [7] M. Gittermann, *J. Phys. A* 34 (2001) L355.
- [8] I. I. Blekhman, P. S. Landa, *Inter. J. Nonl. Mech.* 39 (2004) 421.
- [9] E. Ullner, A. Zaikin, J. Garcia-Ojalvo, R. Bascones, J. Kurths, *Phys. Lett. A* 312 (2003) 348.
- [10] A. A. Zaikin, L. Lopez, J. P. Baltanas, J. Kurths, M. A. F. Sanjuan, *Phys. Rev. E* 66 (2002) 011106.
- [11] V. N. Chizhevsky, G. Giacomelli, *Phys. Rev. A* 71 (2005) 011801.
- [12] J. P. Baltanas, L. Lopez, I. I. Blekhman, P. S. Landa, A. Zaikin, J. Kurths, M. A. F. Sanjuan, *Phys. Rev. E* 67 (2003) 066119.
- [13] E. I. Volkov, E. Ullner, A. Zaikin, J. Kurths, *Phys. Rev. E* 68 (2003) 026214.
- [14] A. O. Maksimov, *Ultrasonics* 35 (1997) 79.
- [15] J. D. Victor, M. M. Conte, *Visual Neuroscience* 17 (2000) 959.
- [16] V. Gheum, N. Zemov, B. Lundborg, A. Vastberg, *J. Atmos. Solar Terrestrial Phys.* 59 (1997) 1831.
- [17] C. W. Cho, Y. Liu, W. N. Cobb, T. K. Henthorn, K. Lillehei, *Pharm. Res.* 19 (2002) 1123.

- [18] J.L.K ames, H W .Burton, Arch.Phys.M ed.Rehabil 83 (2002) 1.
- [19] O .Schlafer, T .Onyecha, H .Borm ann, C .Schroder, M .Sievers, Ultrasonics 40 (2002) 25.
- [20] R .Feng, Y .Zhao, C .Zhu, T J.M ason, Ultrason Sono Chem . 9 (2002) 231.
- [21] G .Baxter, A J.M cK ane, Phys.Rev.E 71 (2005) 011106.
- [22] V M .G andhin athi, K .M urali, S .R ajasekar, Chaos, Solitons and Fractals (2006) (in press).

FIGURES

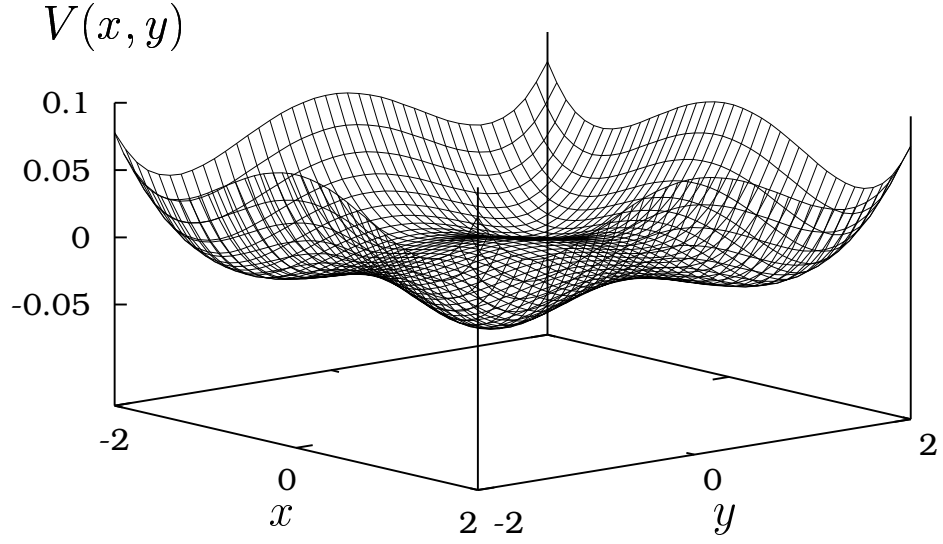


FIG .1. 3-dimensional plot of the potential $V(x, y)$ (eq 2) for the parameters $a_1 = 1.0$, $a_2 = 1.1$, $b_1 = 1.0$, $b_2 = 1.0$, $\epsilon = 0.01$

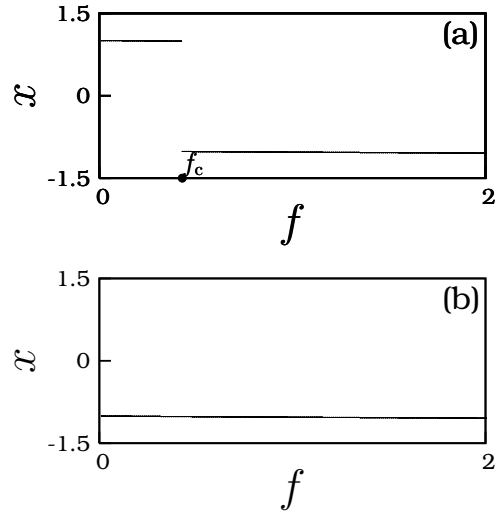


FIG .2. Bifurcation diagrams in the presence of low-frequency force alone. ϵ is set to 0.1. (a) f is varied in the forward direction with the initial condition on the orbit lying in the well V_{++} for the starting value of f . (b) f is varied in the reverse direction from the value 2.

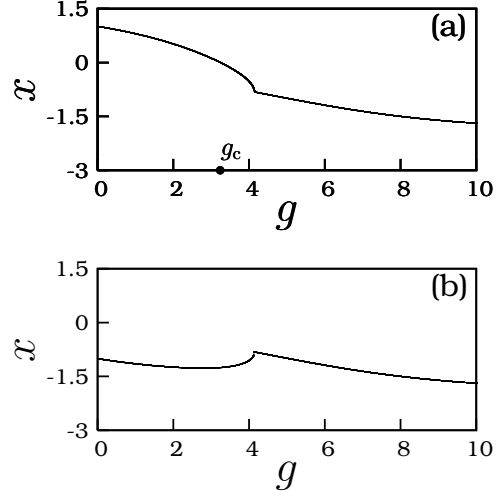


FIG .3. B ifurcation diagram s in the presence of high-frequency force alone. ω is set to 5. (a) g is varied in the forward direction with the initial condition on the orbit lying in the well V_{++} for the starting value of g . (b) g is varied in the reverse direction from the value 10.

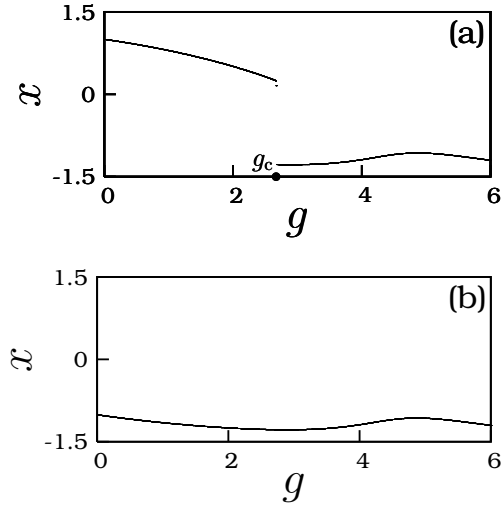


FIG .4. B ifurcation diagram s in the presence of both low-frequency and high-frequency forces. Here $\omega = 0.1$, $\omega_c = 5$ and $f = 0.2$. g is varied in the forward direction in (a) while it is decreased from a large value to small value in (b).

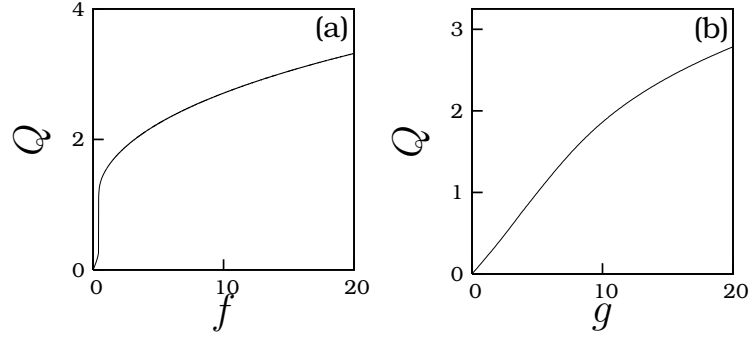


FIG .5. (a) Q versus f where $g = 0$ and $\beta = 0.1$. (b) Q versus g where $f = 0$ and $\beta = 5$.

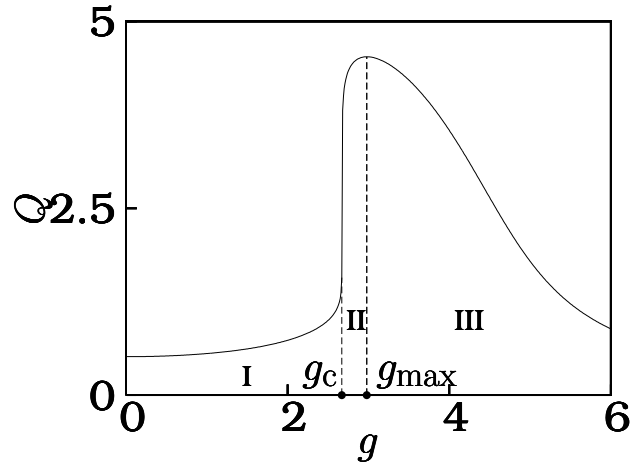


FIG .6. The response amplitude Q versus high-frequency amplitude for the parameters $f = 0.2$, $\beta = 0.1$ and $\gamma = 5$.

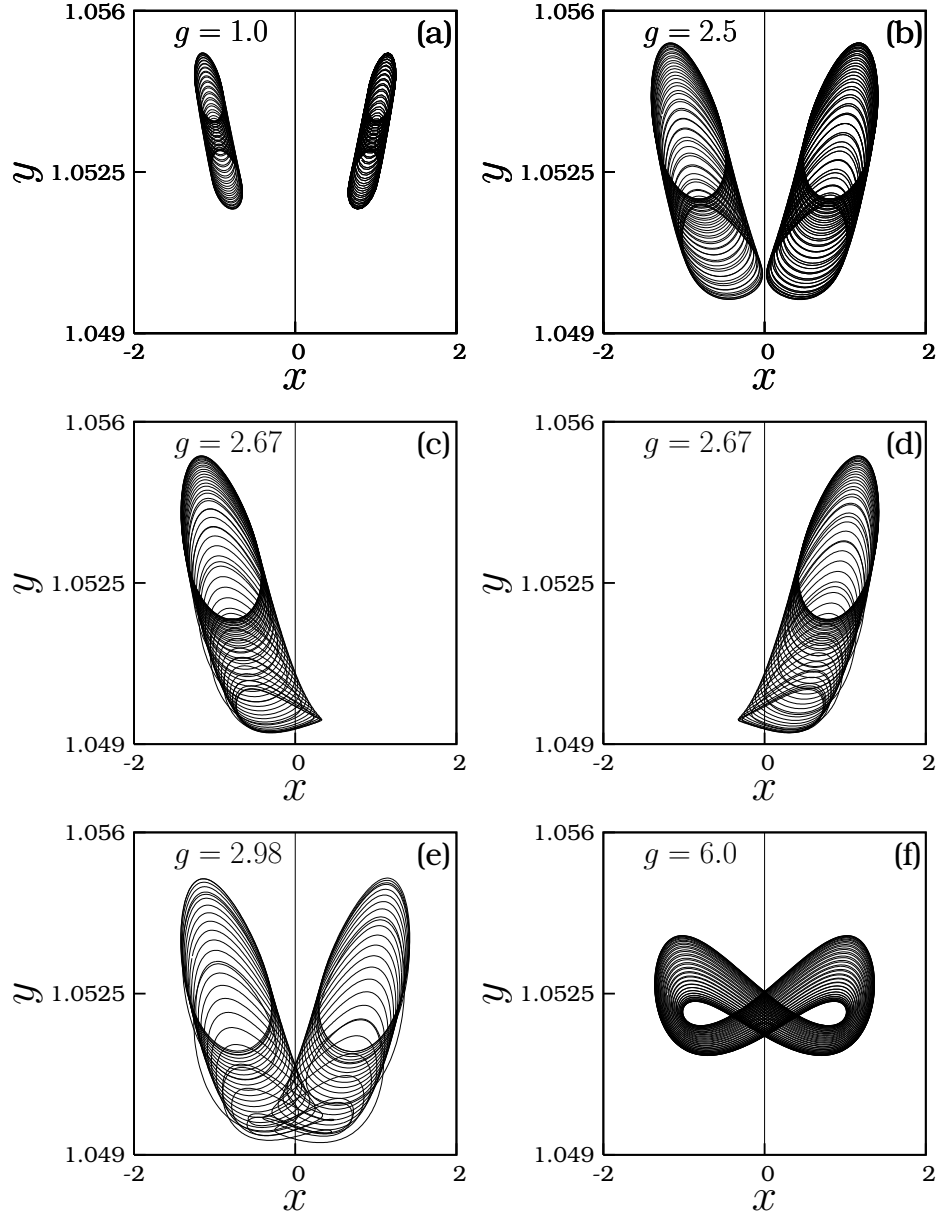


FIG .7. Phase portrait for different values of high-frequency amplitude g . The other parameters are fixed at $f = 0.2$, $\beta = 0.1$ and $\gamma = 5$.

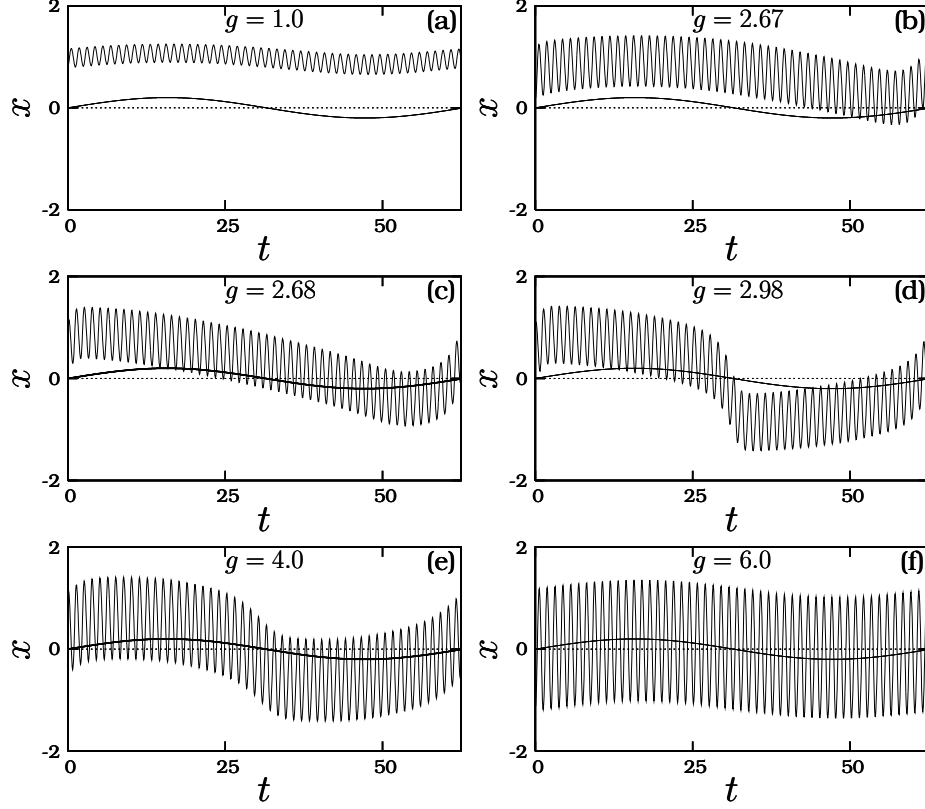


FIG .8. Trajectory plots for few values of g . The parameters are $f = 0.2$, $\lambda = 0.1$ and $\omega = 5$. The low-frequency force is also plotted.

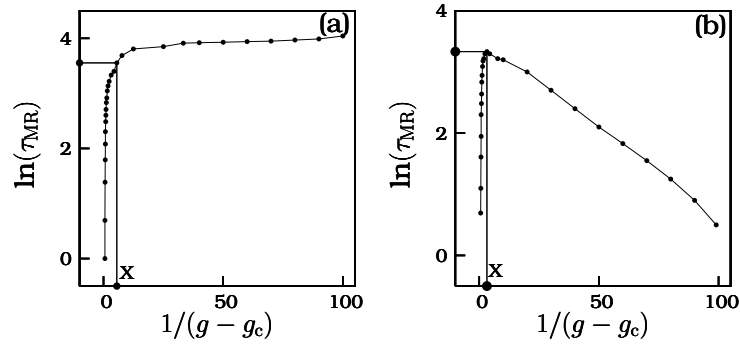


FIG .9. Logarithmic plot of mean residence time of the orbit in the well V_{++} (a) and in the well V_{+-} (b) versus $1/(g - g_c)$.

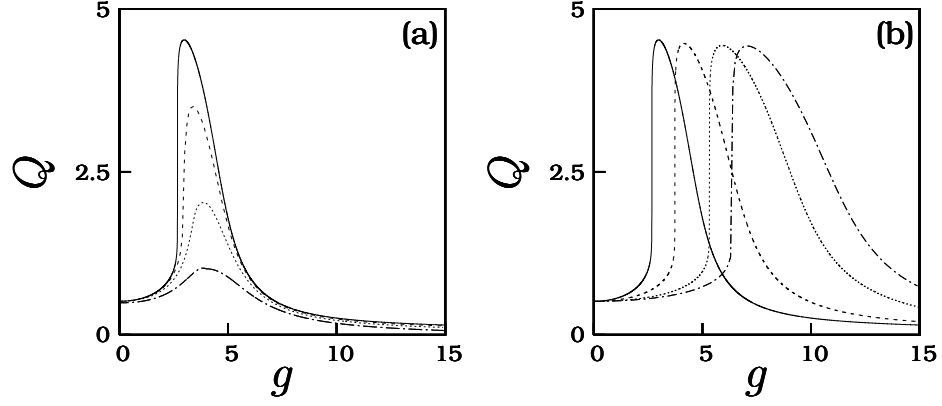


FIG .10. (a) Resonance curves for four fixed values of $!$. From top curve to bottom curve the values of $!$ are 0.1, 0.25, 0.5 and 1.0 respectively. Here $f = 0.2$ and $\gamma = 5$. (b) Resonance curves for four fixed values of γ with $f = 0.2$ and $! = 0.1$. From left curve to right curve the values of γ are 5, 7, 10 and 12 respectively.

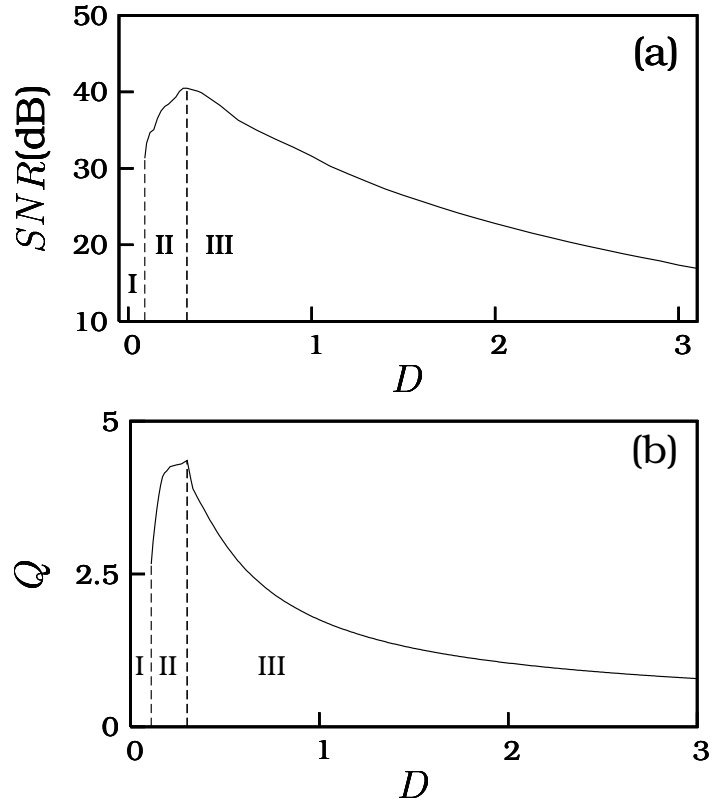


FIG .11. (a) Signal-to-noise ratio plot and (b) Response amplitude plot for a range of noise intensity D with $f = 0.2$ and $! = 0.1$.

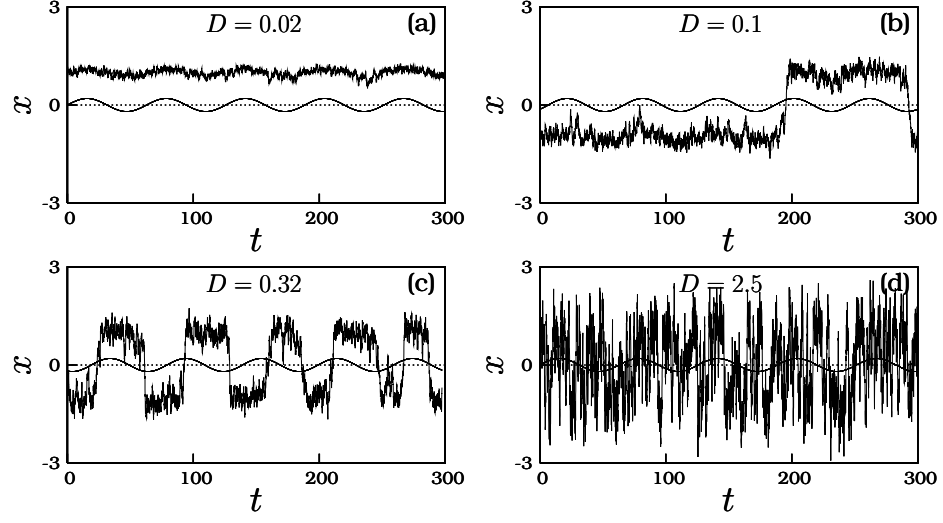


FIG .12. Time series plot for few values of noise intensity D with the system parameters fixed at $f = 0.2, \beta = 0.1$.

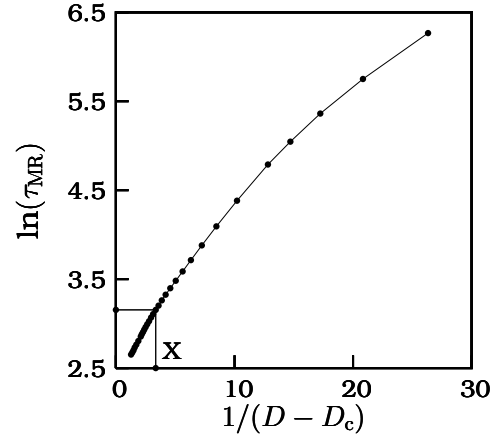


FIG .13. Logarithmic plot of mean residence time against the inverse of $(D - D_c)$. The system parameters are $f = 0.2$ and $\beta = 0.1$. τ_{MR} in V_{++} and V_{-+} are same.